OPEN ACCESS
IOP Publishing
European Journal of Physics
Eur. J. Phys. **44** (2023) 065801 (14pp)
https://doi.org/10.1088/1361-6404/acf0a4

A graduate laboratory experiment to study the dynamics of an acoustically levitated particle

Amit Dolev, Lorenzo Noseda, Bora Yalcin and Mahmut Selman Sakar

Institute of Mechanical Engineering, École Polytechnique Fédérale de Lausanne, Lausanne, Switzerland

E-mail: selman.sakar@epfl.ch

Received 26 April 2023, revised 19 July 2023
Accepted for publication 15 August 2023
Published 5 September 2023

Abstract

The comprehension of physical wave phenomena is imperative for students in the fields of engineering and basic sciences. Laboratory experiments that involve generation of acoustic waves can be used to explain advanced non-linear wave phenomena. Acoustic levitation is a method for stably suspending and trapping objects in mid-air using acoustic radiation forces. This paper discusses an experimental apparatus that offers an economical means to demonstrate the acoustic levitation of polystyrene particles while enabling the investigation of stability and nonlinear dynamics of the trapped particles. Additionally, this platform offers the potential to examine other phenomena, such as the interaction forces between multiple acoustically levitated particles. The mechanical design of the system along with the data acquisition and control techniques are thoroughly explained.

Supplementary material for this article is available online

Keywords: acoustic levitation, graduate laboratory, nonlinear dynamics

(Some figures may appear in colour only in the online journal)

0143-0807/23/065801+14$33.00 Printed in the UK

1. Introduction

The graduate curricula in engineering schools contain multiple physical wave phenomena such as electromagnetics. However, there is generally less focus on acoustics, especially nonlinear acoustics [1]. Nonlinear acoustics deals with situations where the presence of the sound wave has an effect on the properties of the medium through which it propagates. To address this gap, we developed an experimental platform at our institute to demonstrate one of these nonlinear phenomena—standing wave acoustic levitation [2]—and use this platform to characterize nonlinear acoustic forces by studying the dynamics of levitated particles.

Standing wave acoustic levitation is achieved by nonlinear acoustic radiation forces that counteract gravity and trap objects steadily in fluids [2–6]. These forces emerge due to acoustic radiation pressure, which is the pressure impinging upon objects in an acoustic field. The acoustic field is often considered linear, thus the field can be described as a sum of harmonic waves [7]. The acoustic radiation pressure also comprises harmonics, and each harmonic term averages to zero over a cycle, as shown in equation (1)

$$\langle \sin(2\pi f t)\rangle = \frac{1}{T}\int_0^T \sin(2\pi f t)\,\mathrm{d}t = 0, \quad T = \frac{n}{f}, \quad n \in \mathbb{N}. \tag{1}$$

Acoustic levitation occurs due to continuously generated forces, which suggests that the averaged acoustic radiation pressure over a cycle is non-zero. Indeed, due to nonlinear phenomena, the harmonic waves are not pure sinusoids [1, 7]. As a result, the time-averaged acoustic pressure does not cancel out, and the resulting forces acting on small particles can be used to trap them in mid-air [4–6, 8]. The associated nonlinear phenomena are often negligible, but they are significant at high frequencies and high pressure. Acoustic levitators (ALs) are designed to operate at ultrasonic frequencies (i.e. above 20 kHz) and high-pressure levels so that the nonlinear phenomenon is strong enough to enable trapping.

Standing wave ALs are used for contactless handling of delicate specimens to avoid contamination in chemistry [9], microscopy [8], and for the study of organisms in microgravity [10, 11]. They generally require relatively expensive components such as Langevin transducers [12], power amplifiers, and signal generators. Recently, Marzo *et al* introduced TinyLev, a low-cost multi-emitter single-axis AL that operates in air [6]. TinyLev comprises 72 low voltage (20 Vpp) ultrasonic transducers [13] operating at 40 kHz along with 3D printed parts and low-cost electronics. This system is commercially available and can be easily built in a research laboratory, democratizing the study of acoustic levitation. Inspired by the accessibility of TinyLev, we designed an even simpler AL system that works with two transducers.

Graduate students at our institute are provided with a custom-designed platform (figure 1 and video 1) to study acoustic levitation and characterize the dynamics of the problem. They are also asked to explore how the AL can be utilized as a robotic end-effector [5] for high-speed contactless manipulation. ALs have inherent limitations when it comes to the speed of particle manipulation. In our platform, the transducers create axisymmetric acoustic traps as shown in figure 2(a), which apply strong forces in the direction counteracting the gravity (z), whereas the forces in the radial direction (r) are considerably lower (figures 2(b) and (c)). As a result, not to lose the trapped object, the AL must be translated slowly in every direction other than z. To overcome this limitation, an angular degree of freedom (θ) was added to the system in a way that the AL can be rotated and translated (u) (see figures 1 and 3 and video 1).

In section 2, we introduce the underlying theory of acoustic levitation and derive the governing equations of motion for a trapped particle. In section 3, we describe in detail the experimental apparatus and the design of mechanical, optical, and acoustic components. In

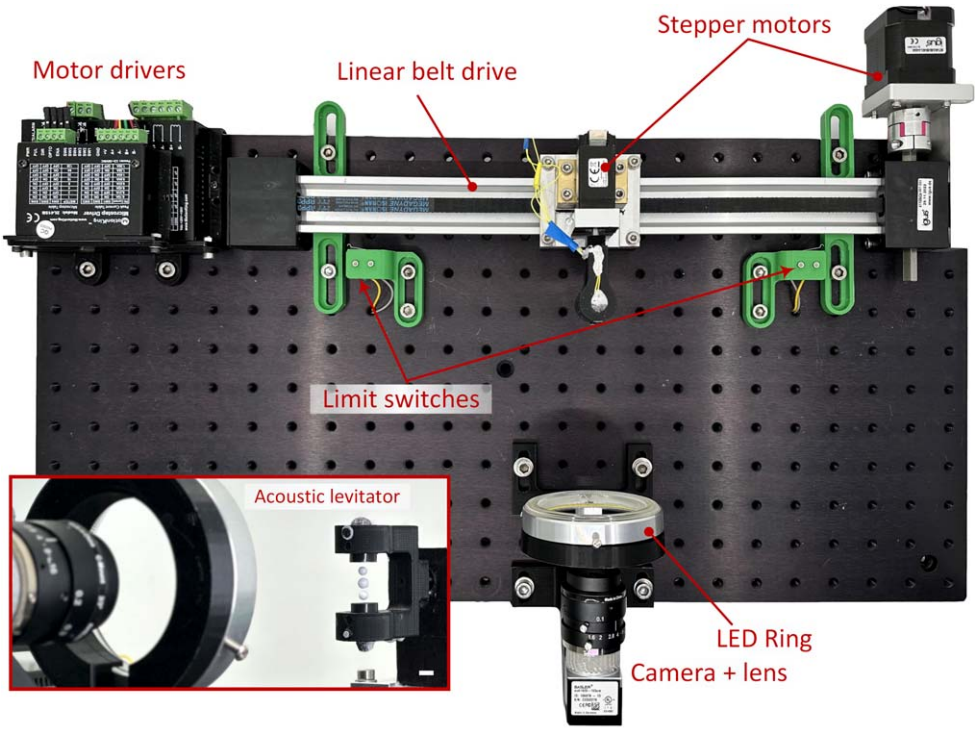

Figure 1. Images of the experimental apparatus showing different mechanical, electronic, and optical components. The scale bar is 5 mm.

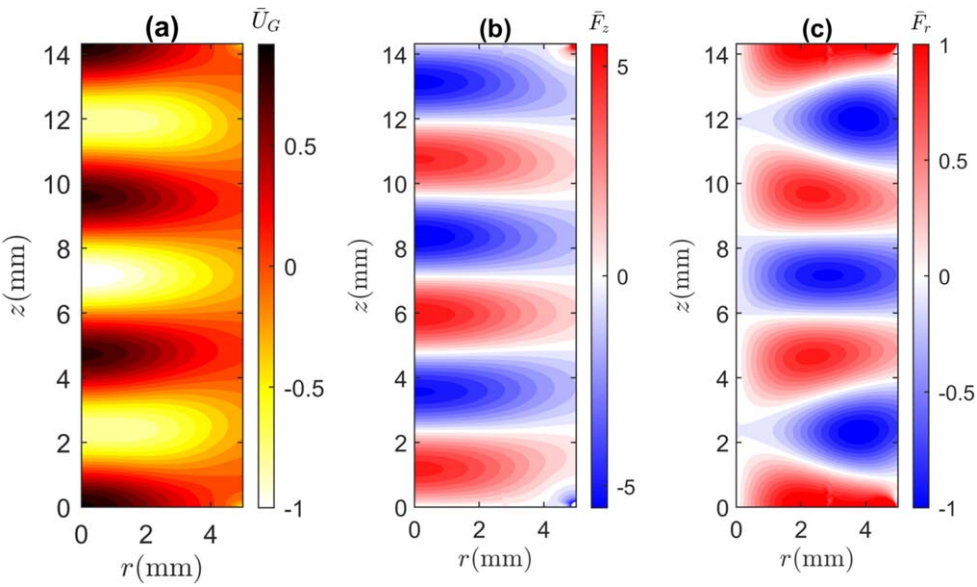

Figure 2. Numerical simulations of the acoustic levitation system excited at 40 kHz. The panels show (a) the axis-symmetric cross-sections of the normalized Gor'kov's potential, and the normalized acoustic radiation forces (b) along z and (c) along r axes.

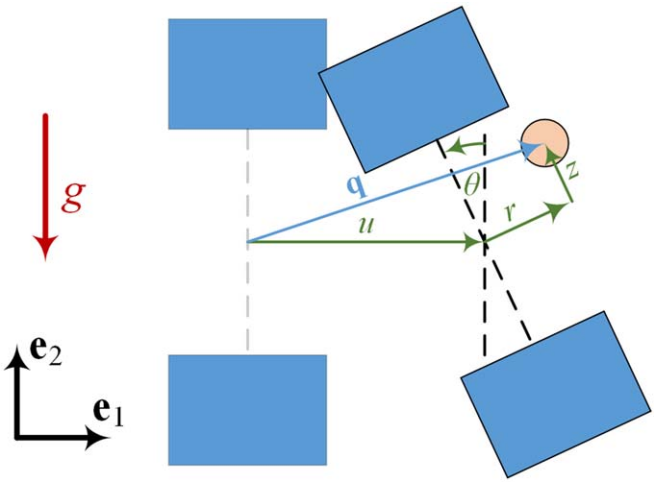

Figure 3. A schematic illustration of the acoustic levitator that is translated and rotated. The peach-colored circle represents the levitated particle, and the green arrows show the coordinate system.

section 4, we provide experimental results demonstrating the characterization of the acoustic trap and the importance of adding a rotational degree of freedom for stable trapping. In the last section, a discussion on future improvements is presented with conclusions drawn from the analysis and results.

2. Theory

2.1. Acoustic radiation forces

Deformable and rigid elements in acoustic fields are subjected to pressure fluctuations due to the acoustic waves impinging their surface. For many applications, the acoustic field can be approximated as linear, thus the acoustic waves can be described by the linear acoustic wave equation. In this case, the acoustic waves are harmonic (i.e. sinusoidal), however, in practice, the field and waves are nonlinear. As a result, the acoustic waves and resulting pressure fluctuations are not symmetric in time, and a net force emerges—acoustic radiation force. To compute the force in the general case, the stress over the surface of the element is integrated, and then time averaged. Further details are provided in supplementary note 1.

Computing the stress and resulting acoustic radiation forces is a complicated task, as one needs to consider the acoustic field, the element geometry, and its movement (i.e. translation, rotation, and deformation). However, for a small rigid spherical particle with a radius significantly smaller than the acoustic wavelength ($a \ll \lambda$) and assuming that the acoustic field consists of standing waves, the forces can be estimated using Gor'kov's theory [14, 15], which was developed for the general case of a compressible sphere. According to the theory, if both the acoustic field in the absence of the sphere, as well as the physical properties of the fluid and the particle, are known, a potential field can be computed. The spatial derivatives of the potential give the acoustic radiation forces acting on the sphere, as follows:

$$\mathbf{F} = -\nabla U_{\mathrm{G}}, \tag{2}$$

where the potential is computed as:

$$U_{\mathrm{G}} = 2\pi a^3\left(\frac{f_1}{3\rho_0 {c_0}^2}\langle {p_1}^2\rangle - \frac{f_2\rho_0}{2}\langle \mathbf{u}_1\cdot\mathbf{u}_1\rangle\right),$$
$$f_1 = 1 - \frac{\rho_0 c_0^2}{\rho_p c_p^2}, f_2 = 2\left(\frac{\rho_p - \rho_0}{2\rho_p + \rho_0}\right). \tag{3}$$

Here a is the radius of the sphere, ρ_0, and ρ_p are the fluid and the sphere densities respectively, c_0 and c_p are the speed of sound in the fluid and sphere respectively, and p_1 and $\mathbf{u}_1$ are the acoustic pressure and acoustic velocity at the center of the sphere when it is not present. The angled brackets operator represents time averaging, similarly to equation (1).

2.2. Nonlinear dynamics—governing equations of motion

To develop the model describing the particle's nonlinear dynamics, we assumed that the particle is subjected to acoustic radiation forces, drag force, and gravity. We neglected the rigid body rotation and acoustic streaming [16, 17], a nonlinear acoustic phenomenon in which mean flow is generated. Considering only the translation and rotation of the AL and using the coordinates as shown in figure 3, the position of the particle is:

$$\mathbf{q} = [u + r\cos(\theta) - z\sin(\theta)]\mathbf{e}_1 + [r\sin(\theta) + z\cos(\theta)]\mathbf{e}_2. \tag{4}$$

The kinetic energy is:

$$T = \frac{m}{2}(\dot{r}^2 + \dot{u}^2 + \dot{z}^2 + 2r\dot{z}\dot{\theta} + [r^2 + z^2]\dot{\theta}^2 + 2\dot{r}[\cos(\theta)\dot{u} - z\dot{\theta}]$$
$$-2\dot{u}\{\dot{z}\sin(\theta) + \dot{\theta}[r\sin(\theta) + \cos(\theta)z]\}), \tag{5}$$

where the overdot represents the derivative with respect to time, and the mass is:

$$m = \frac{4}{3}\pi a^3\rho_p \tag{6}$$

The potential energy including Gor'kov's potential becomes:

$$V = U_{\mathrm{G}}(z, r) + mg[r\sin(\theta) + z\cos(\theta)], \tag{7}$$

where g is the gravitational acceleration, and we modeled the drag force as the drag acting on a smooth sphere:

$$\mathbf{F}_d = -\frac{1}{2}\rho_0\pi a^2\,|\dot{\mathbf{q}}|^2 c_d(\mathrm{Re})\frac{\dot{\mathbf{q}}}{|\dot{\mathbf{q}}|},$$
$$\mathrm{Re} = \frac{|\dot{\mathbf{q}}|\,\rho_0(2a)}{\mu_0}. \tag{8}$$

Here c_d is the drag coefficient [18], which is a function of the Reynolds number (Re) that depends on the particle velocity through the air. Next, using the Lagrange equations, we derived the following equations of motion:

$$\ddot{r} = -\frac{a^2\pi|\dot{\mathbf{q}}|\ \rho_0}{2m}c_d(\mathrm{Re}\,(|\dot{\mathbf{q}}|))(\dot{r} + \cos(\theta)\dot{u} - z\dot{\theta}) + \frac{1}{m}\{m[g\sin(\theta) - \dot{\theta}(2\dot{z} + r\dot{\theta}) + \ddot{u}\cos(\theta) - z\ddot{\theta}] + U_{\mathrm{G},r}\},$$

$$\ddot{z} = \frac{a^2\pi|\dot{\mathbf{q}}|\ \rho_0}{2m}c_d(\mathrm{Re}\,(|\dot{\mathbf{q}}|))(\sin(\theta)\dot{u} - \dot{z} - r\dot{\theta}) - \frac{2}{2m}\{m[g\cos(\theta) + 2\dot{r}\dot{\theta} - z\dot{\theta}^2 - \sin(\theta)\ddot{u} + r\ddot{\theta}] + U_{\mathrm{G},z}\}, \quad (9)$$

where $U_{\mathrm{G},r,}$ and $U_{g,z}$ are the spatial derivatives of Gor'kov's potential with respect to r and z.

3. The experimental apparatus

The experimental apparatus was designed to have a small footprint and operate at relatively low velocities with observable displacements so that the dynamics can be studied without special equipment. The system was designed to operate at a maximum oscillation frequency of 5 Hz not to rely on high-speed imaging. We used a digital camera [19] together with a lens [20], and a low-cost light source [21] to observe the workspace. We processed videos with custom computer vision software to make quantitative measurements of particle motion.

The AL operates at an ultrasonic frequency; thus, the human ear cannot hear the sound. It was designed to generate strong trapping forces in the z-direction and weaker ones in the radial direction. When the apparatus oscillates laterally (u), trapped particles fall under certain conditions, but do not fall when it is simultaneously rotated (θ) at certain velocities, as discussed in section 4.

3.1. The AL

The levitator consists of two low-cost ultrasonic transducers [13] that are excited at 40 kHz. The distance between the two transducers and the phase of the input signal were carefully tuned to generate three acoustic traps as shown in figures 1 and 2. For simplicity, consider a 1D AL, where traveling waves are generated by the transducers (see figure 4). The distance between them and their relative phase, either in phase or out of phase, change the potential field, thus the position of the traps and their existence altogether. The acoustic traps are formed at the pressure nodes of the total pressure field [3], which are located half wavelength, $\lambda/2$, apart. Therefore, for an odd (even) number of traps, the transducer should be spaced apart by an odd (even) number of $\lambda/2$. In addition to the distance, the phase plays an important role, as either constructive or destructive interference occurs leading to either a standing wave (figures 4(b) and (c)) or a perfect cancelation of the pressure field (figures 4(a) and (d)), respectively. To obtain an odd number of traps, the transducers should be excited out of phase (figure 4(b)), while for an even number of traps, they should be excited in phase (figure 4(c)). We designed the AL to have three traps, where the middle trap coincides with the rotation axis.

To set the distance between the transducers, we numerically simulated the acoustic field using commercial software (MATLAB) and an open-source boundary elements method package (OpenBEM [22]). We systematically swept the distance between the transducers, and estimated when the acoustic cavity (i.e. the region between the transducers) is resonating by computing the acoustic power [23]. The results when the transducers are in and out of phase are shown in figure S2. It was numerically found that the optimal distance between the transducers should be 14.3 mm. This result was validated experimentally using a setup where

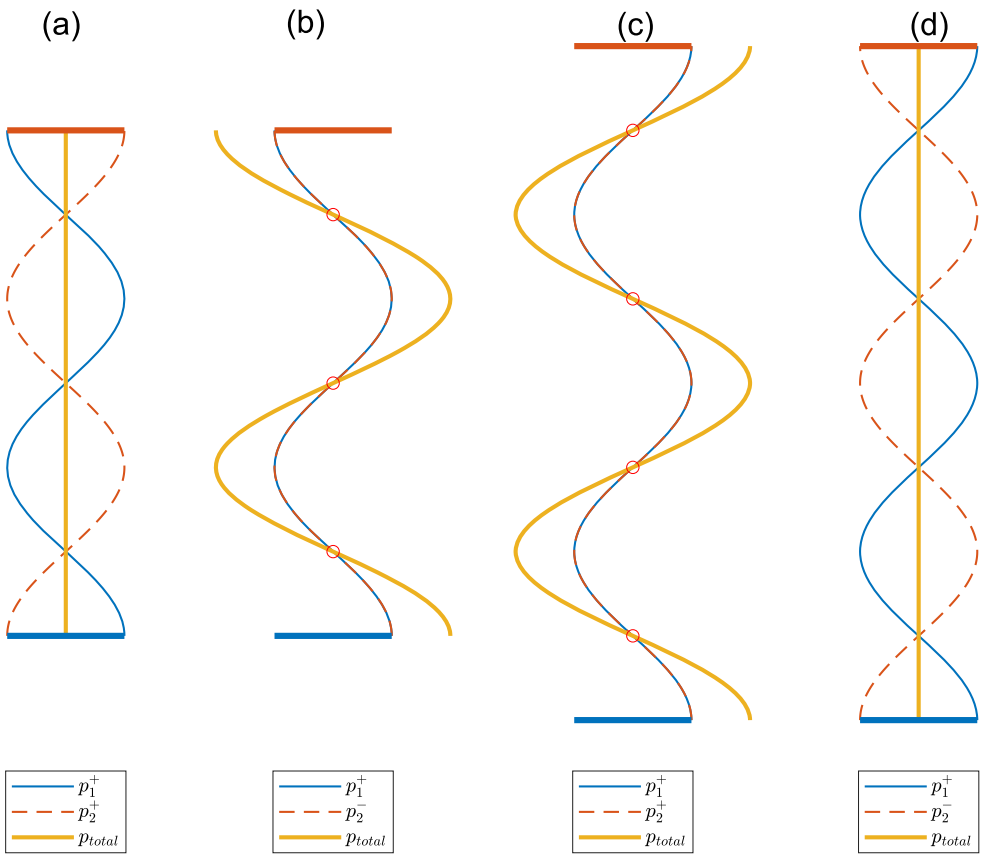

Figure 4. A schematic illustration of the acoustic pressure in the cavity of a 1D acoustic levitator. Each panel shows the pressure fields generated by the bottom (blue), the top (orange dashed) and their sum (yellow) for different cases. The positive (+) and negative (−) superscripts indicate the transducer's phase. (a) The transducers are 1.5 wavelength (λ) apart and they are operated in phase. The system does not generate any traps. (b) The transducers are 1.5 λ apart and out of phase. Three traps are formed inside the cavity. (c) The transducers are 2 λ apart and in phase. Four traps are formed inside the cavity. (d) The transducers are 2 λ apart and out of phase. The system does not generate any traps.

the distance between the transducers could be continuously changed with a linear stage figure S3. The lowest input voltage enabling levitation was registered for different distances, and we found that the optimal distance is 14.8 mm (R.E. of 3.4%). In the final experimental apparatus, the component holding the transducers was 3D printed to have low inertia as discussed in section 3.1.

3.2. The mechanical design

To realize the translational and rotational motion of the AL in a controllable manner, we chose to use a motorized linear belt drive [24], and a small stepper motor [25] (figure 1). For the given inertial loads, the motorized belt drive and stepper motor were chosen to generate the required velocities and accelerations. The stepper motors allow open-loop position control. The micro-stepping drivers [26, 27] enable sufficient smooth motion of 0.0675 mm/step

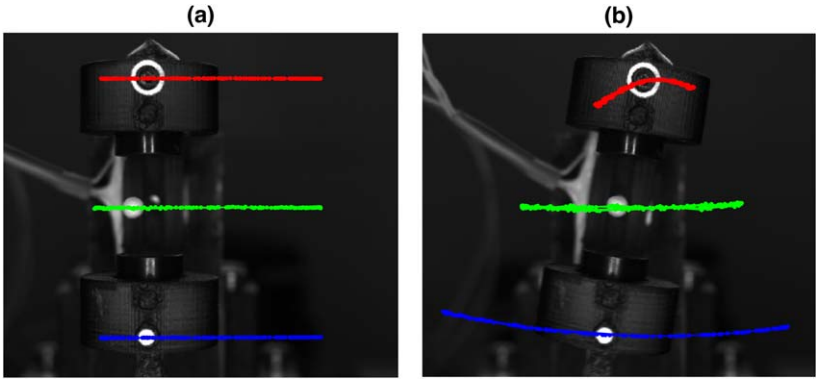

Figure 5. Snapshots from two different levitation experiments, performed without and with rotation. The trajectories of the particle, the bottom marker, and the top marker are shown in green, blue, and red, respectively. (a) The levitation is system is not rotated. (b) The maximum rotation amplitude is set to 28°.

and 0.45 deg/step. The different mechanical components are bolted to an aluminum breadboard [28], which rests on four adjustable feet [29] enabling levelling of the apparatus.

3.3. Control and data acquisition

The system is controlled by a low-cost microcontroller [30], which sends stepping commands to the motor drivers. We mounted limit switches at both ends of the linear stage to stop the system when pressed and move the AL to the center, as a safety measure. The commands are communicated from a PC directly to the microcontroller.

The position and orientation of the AL as well as the particle position are obtained by processing the recorded images. The camera is calibrated using the MATLAB Camera Calibration application of the Computer Vision Toolbox to obtain the camera parameters and the pixel-to-mm ratio. The particle and markers on the AL are tracked using a subpixel image registration algorithm [31]. Figures 5 and S6 show examples of processed videos and tracking of features.

4. Experimental results

Characterizing the acoustic trap is a crucial step that is required to understand the particle dynamics. To do so, one may consider measuring the acoustic field directly with a microphone; however, it is not a trivial task. It requires a microphone with high sensitivity at 40 kHz that has a small size not to interfere with the field ($d \ll \lambda \approx 8.6$ mm) and a high-resolution 3D positioning system. Alternatively, an opto-acoustical computational tomography method can be used [32]. However, this method requires a unique setup and expensive equipment such as a laser Doppler vibrometer [33]. To provide a practical solution for the graduate laboratories, we relied on numerical simulations of the acoustic field topology, and hence the trapping forces (figures 2(b) and (c)).

To estimate the forces, we measured the static displacement (r_s, z_s) of Styrofoam particles with known radii and density (31 kg m^{-3}) for different voltage values, where the potential is proportional to the input voltage squared, V^2 [4]. From equation (9), the particle should satisfy the following equations

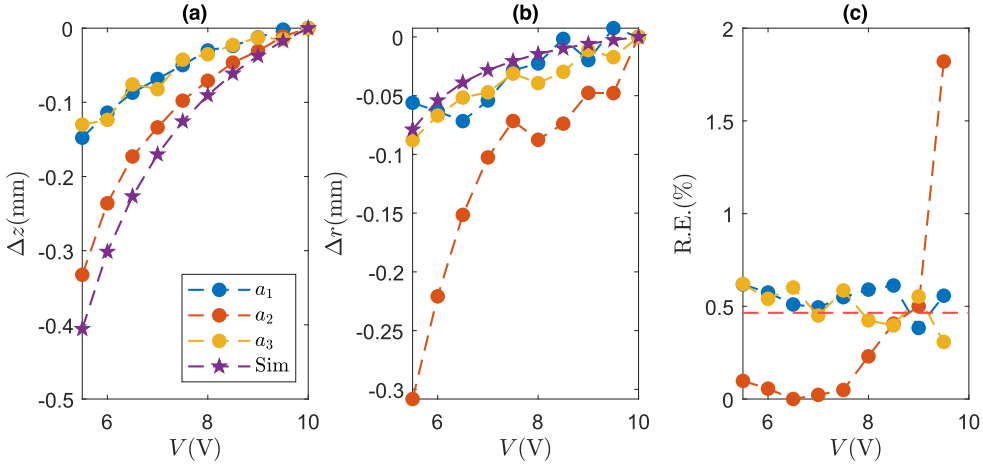

Figure 6. Experimental and simulated data showing the relative positions of three different particles ($a_1 = 1.59$ mm, $a_2 = 1.83$ mm, $a_3 = 1.45$ mm). The positions of the particles (a) along z and (b) along r axes with respect to the input voltage. (c) The relative Euclidian distance error between the experimental data and numerical simulations that were computed with the optimal Gor'kov potential.

$$V^2 \alpha U^N_{\mathrm{G},r}(r_s, z_s) = mg \sin(\theta), \quad V^2 \alpha U^N_{\mathrm{G},z}(r_s, z_s) = -mg \cos(\theta). \tag{10}$$

where U^N_{G} is the numerically computed Gor'kov potential, and it is assumed to be proportional to the actual potential, (i.e. $\alpha U^N_{\mathrm{G}} = U_{\mathrm{G}}$). The static displacements, angle θ, mass m, and voltage can be experimentally measured, and compared to numerical simulations to estimate α and obtain U_{G}. This was done by solving an optimization problem in MATLAB using the Optimization Toolbox. The following cost function was minimized:

$$\min_{\alpha} \frac{1}{N} \sum_{i=1}^{N} \mathrm{R.E.}^i, \ \mathrm{R.E.}^i = \left| \frac{\Delta_i^{\mathrm{sim}} - \Delta_i^{\mathrm{exp}}}{\Delta_i^{\mathrm{sim}}} \right|, \tag{11}$$

where

$$\begin{aligned} \Delta_i^{\mathrm{sim}} &= \sqrt{[r^{\mathrm{sim}}_{10V} - r^{\mathrm{sim}}(V_i)]^2 + [z^{\mathrm{sim}}_{10V} - z^{\mathrm{sim}}(V_i)]^2}, \\ \Delta_i^{\mathrm{exp}} &= \sqrt{[r^{\mathrm{exp}}_{10V} - r^{\mathrm{exp}}(V_i)]^2 + [z^{\mathrm{exp}}_{10V} - z^{\mathrm{exp}}(V_i)]^2}. \end{aligned} \tag{12}$$

The exact position of the trap in the image plane is unknown; therefore, we chose to minimize the difference between the position distances for different voltage values, and not the absolute position. After the estimation process of α, for particles with radii of 1.59, 1.83 and 1.45 mm, the numerically simulated and measured static deflections for different voltage values are shown in figures 6 and S4. The agreement is satisfactory, and it captures the nature of the problem. One of the reasons for the discrepancies is the deviation from the theory. According to the theory, the sphere's radius should be much smaller than the acoustic wavelength, whereas here $\lambda/a \approx 5$. This is clearly visible from the data that was used to estimate α (figure S4) because particles with different radii and the same density should settle in the same position, as computed in the simulations. This is because spherical particles are subjected to acoustic forces and gravitational forces that are proportional to their volume, according to the theory (equation (3)). It is interesting to note that because the cost function

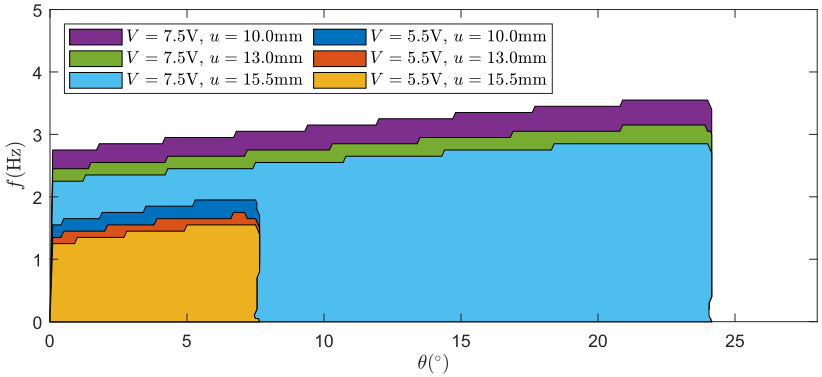

Figure 7. Numerically computed stability charts, when the translation (u) and rotation (θ) are in phase for different parameters. The colored regions indicate stable motion.

(see equation (11)) was defined as an average of the experiments, the largest particle ($a_2 = 1.83$ mm) influenced the fitting the most.

To conclude this section, discrepancies between the theory and the experiments are expected, and the hybrid method to estimate and calibrate the acoustic trap proved to be sufficient. In the following part, the students are encouraged to explore strategies to take advantage of the trap topology to translate the particle faster, without dropping it.

4.1. Stable translation schemes

According to the dynamic model given in equation (9), we can estimate the forces leading to the particle's escape from the trap. For simplicity, we consider only harmonic translation (i.e. $\theta = 0$) up to 5 Hz, and a Styrofoam particle with a radius of 1.5 mm. Figure S5 depicts the ratio of the inertia to the drag force for different frequencies and amplitudes. For the considered values, inertia is the leading reason for the escape of the particle. After calibrating the numerical model, we simulated the system to examine different scenarios and developed schemes for fast and stable translation. We numerically studied the stability of a 1.5 mm radius Styrofoam particle at different input voltages, translational amplitudes, and rotational amplitudes when the translation and rotation are in phase. Figure 7 depicts the stable and unstable regions for input voltages of 5.5 and 7.5 V and translational amplitudes of 10, 13, and 15.5 mm for different frequencies and rotational amplitudes. It can be seen that adding rotation can increase the stability at higher frequencies, therefore higher velocities and accelerations. As discussed in section 4, there are discrepancies between the experimental data and theory, therefore, only a qualitative match between the experiments and simulation results is feasible.

We considered the case where the rotation and translation are in phase and studied the stability for various frequencies and amplitudes. We experimentally showed that it is possible to keep a particle inside the trap by adding rotation. Figure 5 depicts snapshots from two different experiments where the AL is only translated or simultaneously translated and rotated (video 2). The images were processed to extract the position and orientation of the AL along with the position of the particle. In both experiments, the translational amplitude was set to 15.4 mm, and the voltage to 5.5 V. Without rotation (figure 5(a)) the particle escaped the AL at frequencies higher than 2.6 Hz. By adding rotation ($\theta \approx 28^\circ$), the maximum stable frequency was increased to 3.32 Hz, corresponding to an increase of 27.7%. We repeated the

Table 1. Data collected from levitation experiments at varying translational and rotational amplitudes.

Voltage (V)	Translational amplitude (mm)	Rotational amplitude (°)	Maximum stable frequency (Hz)	Improvement (%)	Maximum velocity (ms^{-1})	Maximum acceleration (ms^{-2})
5.5	15.4	0	2.60	27.7	0.25	4.11
		28	3.32		0.32	6.70
	12.8	0	2.83	24.7	0.23	4.05
		28	3.53		0.28	6.30
	10.3	0	3.01	33.5	0.19	3.68
		28	4.02		0.26	6.57

experiment for amplitudes of 12.8 and 10.3 mm, and the results are provided in table 1. As expected, adding rotation allows translating the particle faster, by about 28% on average. In addition, without rotation, the particle falls for accelerations higher than $3.9 \pm 0.2\,\mathrm{ms}^{-2}$ independent of the velocities that are on the same order ($0.26 \pm 0.04\,\mathrm{ms}^{-1}$), which indicates that the particle leaves the trap due to its inertia and not air drag. The particle escapes the trap when the acceleration is maximal (video 3). The trajectory of a representative particle escaping the trap is shown in figure S6.

5. Discussion and conclusions

The presented experimental platform aims to expose graduate students to advanced concepts in acoustics, especially nonlinear acoustics and acoustic radiation forces. These forces can be harnessed to design an AL end-effector, a device capable of manipulating small rigid particles without contact. The setup was designed to demonstrate the intricate nonlinear dynamics of an acoustically levitated spherical particle while avoiding advanced nonlinear dynamic phenomena such as parametric resonance [4, 34] and acoustic streaming [17]. Moreover, it was designed to be interactive and relatively slow so that the phenomena can be observed without unique measuring equipment. Throughout the experiment, the students learn how to estimate the acoustic field, through numerical simulations and proxy measurements. In addition, the students learn about the limitations of the analytical model and the importance of calibration by observing the discrepancies between the equilibrium positions of different particles (figures 6 and S4).

After calibration, the nonlinear dynamics of the particle motion is studied numerically, which enables the development of schemes to translate the AL faster without dropping the particle. Here, we only demonstrated the case where the rotation and translation are in phase, and at the same frequency. However, other schemes are possible, such as rotating the AL in phase with the translation at a frequency that is an odd multiplication of the translation frequency. It was also found experimentally that the forces leading to the particle's escape are mostly inertial (figure S6 and table 1).

This platform can be used to study more advanced phenomena, such as the interaction between acoustically levitated particles [35], as it enables levitating of up to three particles simultaneously (see figure 1). In addition, it can be used to teach tuneable oscillators, as the stiffness of the trap can be modulated by changing the input voltage, while the mass remains the same. Alternatively, the stiffness can be changed by rotating the AL. Harmonic base excitation can be explored as well, as it can be introduced to the system by the translational oscillation of the AL. Furthermore, characterizing the acoustic field or the three different traps can be done by estimating the resonances of trapped spheres [4].

Acknowledgments

This project has received funding from the European Union's Horizon 2020 research and innovation program under the Marie Sklodovska-Curie, Grant Agreement No. 101022448. We would like to thank Izhak Bucher and Elad Tenenbaum for their assistance with the control system and fruitful discussions, and the members of the Microbiorobotic Systems (MICROBS) Laboratory for their intellectual feedback.

Data availability statement

Beyond the experimental data, which are provided in the form of videos, additional data include CAD designs of the system, C code for the specific microcontroller, and MATLAB scripts [36].

Disclosures

The authors declare that there are no conflicts of interest related to this article.

ORCID iDs

Amit Dolev https://orcid.org/0000-0003-1540-9784
Lorenzo Noseda https://orcid.org/0009-0006-7134-7118
Mahmut Selman Sakar https://orcid.org/0000-0002-7226-3382

References

[1] Hamilton M F and Blackstock D T 1998 *Nonlinear Acoustics* (Academic Press)
[2] Zang D 2020 *Acoustic Levitation* (Singapore: Springer) (https://doi.org/10.1007/978-981-32-9065-5)
[3] Andrade M A B, Pérez N and Adamowski J C 2018 Review of progress in acoustic levitation *Braz. J. Phys.* **48** 190–213
[4] Dolev A, Davis S and Bucher I 2019 Noncontact dynamic oscillations of acoustically levitated particles by parametric excitation *Phys. Rev. Appl.* **12** 034031
[5] Ezcurdia I, Morales R, Andrade M A B and Marzo A 2022 LeviPrint: contactless fabrication using full acoustic trapping of elongated parts *Special Interest Group on Computer Graphics and Interactive Techniques Conf. Proc. (SIGGRAPH '22 Conf. Proc.), August 7â•fi11, 2022* vol 1 *(Vancouver, BC, Canada)* (Association for Computing Machinery (ACM)) pp 1–9
[6] Marzo A, Barnes A and Drinkwater B W 2017 TinyLev: a multi-emitter single-axis acoustic levitator *Rev. Sci. Instrum.* **88** 085105
[7] Pierce A D 2019 *Acoustics: An Introduction to its Physical Principles and Applications* (Springer International Publishing)
[8] Helander P, Puranen T, Meriläinen A, Maconi G, Penttilä A, Gritsevich M, Kassamakov I, Salmi A, Muinonen K and Hæggström E 2020 Omnidirectional microscopy by ultrasonic sample control *Appl. Phys. Lett.* **116** 194101
[9] Zheng Y, Zhuang Q, Ruan Y and Wei B 2023 Acoustic levitation synthesis and subsequent physicochemical properties of bimetallic composite nanoparticles *Appl. Phys. Lett.* **122** 084102
[10] Xie W J, Cao C D, Lü Y J, Hong Z Y and Wei B 2006 Acoustic method for levitation of small living animals *Appl. Phys. Lett.* **89** 214102
[11] Li L, Gu N, Dong H, Li B and Kenneth T V G 2020 Analysis of the effects of acoustic levitation to simulate the microgravity environment on the development of early zebrafish embryos *RSC Adv.* **10** 44593–600
[12] Moreno E, Acevedo P, Fuentes M, Sotomayor A, Borroto L, Villafuerte M E and Leija L 2005 Design and construction of a bolt-clamped Langevin transducer *2nd Int. Conf. on Electrical and Electronics Engineering, ICEEE and 11th Conf. on Electrical Engineering, CIE 2005* vol 2005, pp 393–5
[13] Murata Manufacturing 2023 Ultrasonic sensor part number MA40S4S (www.murata.com/en-eu/products/productdetail?partno=MA40S4S)
[14] Gor'kov L P 1962 On the forces acting on a small particle in an acoustical field in an ideal fluid *Sov. Phys.-Dokl.* **6** 773–5
[15] Bruus H 2012 Acoustofluidics 7: the acoustic radiation force on small particles *Lab Chip* **12** 1014–21

[16] Boluriaan S and Morris P J 2003 Acoustic streaming: from rayleigh to today *Int. J. Aeroacoustics* **2** 255–92
[17] Hasegawa K, Abe Y, Kaneko A, Yamamoto Y and Aoki K 2009 Visualization measurement of streaming flows associated with a single-acoustic levitator *Microgravity Sci. Technol.* **21** 9–14
[18] Morrison F A 2013 *Data Correlation for Drag Coefficient for Sphere* (Houghton, MI: Department of Chemical Engineering, Michigan Technological University) (https://pages.mtu.edu/~fmorriso/DataCorrelationForSphereDrag2016.pdf)
[19] Basler 2023 Digital camera part number acA1920-155 μm (https://baslerweb.com/en/products/cameras/area-scan-cameras/ace/aca1920-155um/)
[20] Basler 2023 Lens part number C23-1216-2M-S f12 mm (https://baslerweb.com/en/products/cameras/area-scan-cameras/ace/aca1920-155um/)
[21] Adafruit 2023 LED ring light—76 mm diameter (https://adafruit.com/product/4433)
[22] Cutanda Henriquez V and Juhl P M 2010 OpenBEM—an open source boundary element method software in acoustics *Internoise 2010* pp 5796–805
[23] Xie W J and Wei B 2002 Dependence of acoustic levitation capabilities on geometric parameters *Phys. Rev.* E **66** 026605
[24] Igus 2023 Motorized linear belt drive part number ZLW-0630-Eco (https://igus.com/info/news-2015-us-14903)
[25] Joy-it 2023 Stepper motor part number NEMA08-02 (https://joy-it.net/en/products/NEMA08-02)
[26] MotionKink 2023 Micro-stepping motor dirver part number 2L415B (http://motionking.com/Products/Drivers/stepper_motor_drivers.htm)
[27] MotionKink 2023 Micro-stepping motor dirver part number 2LD545 (http://motionking.com/Products/Drivers/stepper_motor_drivers.htm)
[28] THORLABS 2023 Aluminum Breadboard part number MB3045/M (https://thorlabs.com/thorproduct.cfm?partnumber=MB3045/M)
[29] THORLABS 2023 Breadboard mounting feet part number BMF4/M (https://thorlabs.com/thorproduct.cfm?partnumber=MB3045/M)
[30] STMicroelectronics 2023 STM32 Nucleo-64 development board part number Nucleo-G474RE (https://st.com/en/evaluation-tools/nucleo-g474re.html)
[31] Guizar-Sicairos M, Thurman S T and Fienup J R 2008 Efficient subpixel image registration algorithms *Opt. Lett.* **33** 156–8
[32] Tenenbaum E and Bucher I 2022 Reconstruction of a nonlinear acoustic field based on acousto-optic effect computational tomography *ISMA 2022—Int. Conf. on Noise and Vibration Engineering*
[33] Yatabe K, Ishikawa K and Oikawa Y 2017 Acousto-optic back-projection: physical-model-based sound field reconstruction from optical projections *J. Sound Vib.* **394** 171–84
[34] Sugita N, Oshino T and Shinshi T 2023 Nonlinear coupling between radial and axial vibrations during single-axis acoustic levitation in mid-air *Int. J. Mech. Sci.* **246** 108159
[35] Hasegawa K and Murata M 2022 Oscillation dynamics of multiple water droplets levitated in an acoustic field *Micromachines* **13** 1373
[36] Dolev A and Noseda L 2023 Acoustic Levitation apparatus *Robotics Practicals*